A Design of Fractional-slot Concentrated Winding IPM Synchronous Motor for Electric Vehicles

Ding Zuopeng, Zhang Bing, Yin Dejun
School of Mechanical Engineering
Nanjing University of Science and Technology
Nanjing, Jiangsu, China
Email: yin@njust.edu.cn

***Abstract*—This paper presents the design of an interior permanent magnet synchronous motor (IPMSM) with fractional-slot concentrated winding (FSCW). The study determines the number of poles and slots considering the winding factor and unbalanced magnetic force. Conventional calculation method is used to obtain the initial dimensions and finite element analysis (FEA) is adopted to acquire the performance of the motor. The study optimizes the rotor structure, adjusting the eccentric length and the angle of pole shoe, so as to improve the torque quality. Finally, the finite element results verify the effectiveness of the optimization.**

Keywords—design; interior permanent magnet synchronous motor; fractional-slot concentrated winding; torque quality; rotor structure.

I. INTRODUCTION

Facing the challenges of energy crisis and environmental pollution, electric vehicles (EVs) have been gaining popularity and gradually replacing the conventional cars. However, the performance requirements for electric vehicle motors are complicated, such as constant torque characteristics, high overload multiples of torque, low torque fluctuation and light weight. IPMSM is especially suitable for automotive applications [1] on account of its superior performance of high torque density, high power density, high power factor, and high efficiency [2]. The winding form of permanent magnet motor usually has two types: distributed winding and concentrated winding. Compared to the distributed winding motor, the concentrated winding motor presents shorter end-winding length, higher fill factor, lower cogging torque, better fault tolerance and other significant advantages [3], [4]. FSCW-IPMSM has been gaining interest over the last few years.

Different with the surface-mounted permanent magnet synchronous motor (SPMSM), the electromagnetic torque of IPMSM consists of two components. One is permanent magnet torque and the other is reluctance torque. The reluctance torque is caused by the asymmetry of magnetic circuit of d-axis and q-axis and its value is related to saliency ratio, which represents ratio of q-axis inductance to d-axis inductance [5]. Higher saliency ratio produces greater reluctance torque. Furthermore, the motor with a certain rate of salient is suitable for sensor-less control. However, if a concentrated-winding stator is used for IPMSM, the saliency ratio is less than that of IPMSM with a distributed winding [6]. Therefore, variation of saliency ratio is a concern when optimizing the FSCW-IPMSM.

For EVs, it is necessary to reduce the pulsating torque of the driving motors. In generally, the methods of suppressing pulsating torque are divided into two paths. The first one focuses on the optimization of control method, which uses various complicated strategies to eliminate or compensate the torque pulsation [7]. The second one is based on the optimization design of motor body, which is issue of this study.

The pulsating torque is mainly related to the following four aspects: 1) cogging torque; 2) ripple torque due to back electromotive force (Back-EMF) waveform harmonics; 3) reluctance torque; 4) magnetic saturation [8]. Among them, the cogging torque has been studied most extensively and many methods were put forward, such as pole-arc coefficient optimization [9], rotor pole face optimization [10], stator skewing or rotor step (discrete) skewing [11] and so on. However, methods to reduce the pulsating torque caused by one aspect can also affect the other performance. For instance, the stator or rotor skewing also reduces the Back-EMF waveform harmonics and decreases the ripple torque [8], [12]. Reluctance torque not only affects the pulsating torque, but also contributes to increasing the output torque. Therefore, it's important to consider the variety of multiple performance in the process of motor optimization.

The aim of this paper is to design a FSCW-IPMSM for EV applications. In section II, according to design requirements, the initial model is determined, including its number of poles and slots and main dimensions. The performance is obtained by finite element analysis. Section III optimizes the rotor structure, including the eccentric length and the angle of pole shoe. Finally, some conclusions are presented in section IV.

II. INITIAL DESIGN OF PERMANENT MAGNET MOTOR

A. Selection of the number of poles and slots

According to the basic theory of winding, number of slots per pole of each phase q can be given as

$$q = \frac{Q}{2pm} \tag{1}$$

978-1-5386-1127-2/17/$31.00 ©2017 IEEE

where Q represents the number of slots, p is the number of pole-pairs and m is the number of phases. For fractional-slot concentrated winding permanent motor, q is a fraction and winding pitch is 1.

The winding factor K_{dp} is an important factor to be considered when determining the number of poles and slots. It shows the utilization of windings and is directly proportional to the motor Back-EMF and output torque. Thus, the goal is to get a winding factor with a high value. Table I shows the poles and slots combinations which the winding factors are more than 0.9 and the numbers of poles are less than 20. Too many poles require excessive current frequency and result in excessive iron loss.

Improper selection of the number of poles and slots will result in uneven distribution of the magnetic flux of the stator windings and produce unbalanced magnetic force. In order to effectively suppress the unbalanced magnetic force, the study sets the poles' number to 16 and the slots' number, 18. The motor consists of two 8 poles -9 slots unit motors.

B. *Determination of main dimensions*

Basic dimensions of the motor can be estimated from [13]

$$T_e = \frac{\sqrt{2}\pi}{4} k_{dp} B_{\delta 1} A L_{ef} D_{i1}^2 \cos\gamma \tag{2}$$

$$P_o = \frac{\sqrt{2}\pi^2}{2r} k_{dp} D_{i1}^2 L_{ef} n_s B_{\delta 1} A \eta \cos\varphi \tag{3}$$

where T_e represents the electromagnetic torque, $B_{\delta 1}$ is the fundamental amplitude of air gap magnetic flux density, A is the effective value of stator electric load, L_{ef} is the axial length of the machine, D_{i1} is the stator inner diameter, γ is the angle between the phase current and Back-EMF, P_o is the output power, r is the ratio of Back-EMF to the phase voltage, n_s is the synchronous speed, φ is the power factor angle and η is the efficiency.

Table II shows the main requirements of the permanent magnet motor. The cooling method of motor adopts natural air cooling. Taking into account the temperature rise and structure size, the predicted value of $B_{\delta 1}$ and A is set to 0.875T and 21A/mm respectively under rated load. Air gap length is another important factor to be pondered. Smaller air gap length is beneficial to engender higher air gap flux density and obtain higher utilization rate of permanent magnet, but it is limited by processing technic and assembly process. This study sets the air gap length to be 0.8mm. According to the requirements, main parameters are estimated and shown in Table III. Fig. 1 shows the established 2D model.

C. *Performance of the initial design*

After determining the initial model, the performance of the motor is obtained by FEA. 50W470 is selected to be the stator and rotor material mainly considering the cost. The temperature has great influence on the performance of permanent magnet. Thus, the study set the permanent magnet material to be N42SH to ensure the electromagnetic performance of the motor. Fig. 2 shows the B-H curves of N42SH at different temperatures. In order to reduce the difference between the FEA results and the actual performance, the temperature of permanent magnets is set to 80 °C.

TABLE I. WINDING FACTORS

Poles and Slots	Winding Factor	Poles and Slots	Winding Factor
8P9S	0.945	14P15S	0.951
10P9S	0.945	14P18S	0.902
10P12S	0.933	16P15S	0.951
14P12S	0.933	16P18S	0.945

TABLE II. MAIN REQUIREMENTS OF IPMSM

Parameters	Value	Parameters	Value
Peak Power	21kW	Peak Torque	160Nm
Rated Power	10kW	Rated Torque	64Nm
Maximum Speed	5000rpm	Bus Voltage	288V
Maximum outer diameter	260mm	Minimum inner diameter	>150mm
Length of Machine	<100mm	Torque Ripple	<5%

TABLE III. MAIN PARAMETERS OF IPMSM

Parameters	Value	Parameters	Value
Outer Diameter of Stator	260mm	Inner Diameter of Stator	200mm
Length of Machine	80mm	Air Gap	0.8mm
PM Width	13.2mm	PM Thickness	5.5mm
Tooth Width	15mm	Core Width	9.5mm

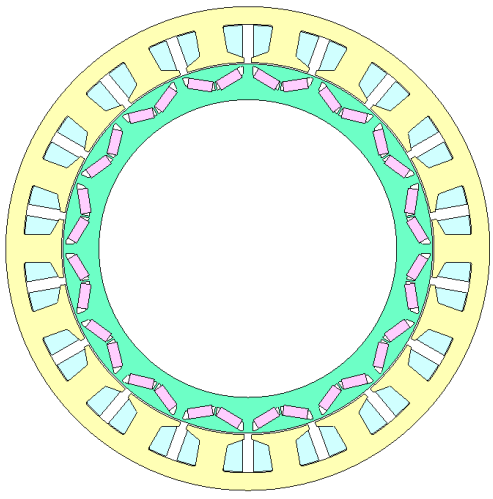

Fig. 1. Established 2D model of the initial motor

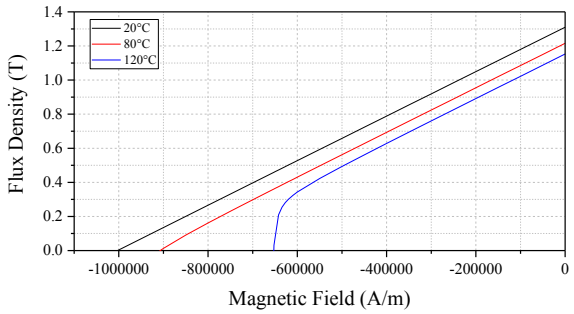

Fig. 2. B-H curves of N42SH at different temperatures

Fig. 3 shows the air gap flux density waveform of the established model. The fundamental amplitude is 0.832T, less than the predicted value after Fourier analysis. Accordingly, the fundamental amplitude of max Back-EMF is 158.45V, less than 166.28V. Fig. 4 shows the Back-EMF waveforms of a period.

Fig. 5 shows the torque versus speed diagram under the max load and rated load. Though the air gap flux density is smaller, the output torque basically meets the requirements for the influence of reluctance torque. Fig. 6 and Fig. 7 show the cogging torque and output torque waveforms. The cogging torque amplitude is 0.145Nm. The pulsating torque of the max torque and rated torque are 10.86Nm and 3.63Nm, up to 6.97% and 5.64% of the output torque respectively. Compared with the output torque, the cogging torque is small enough and it is ignored in this study.

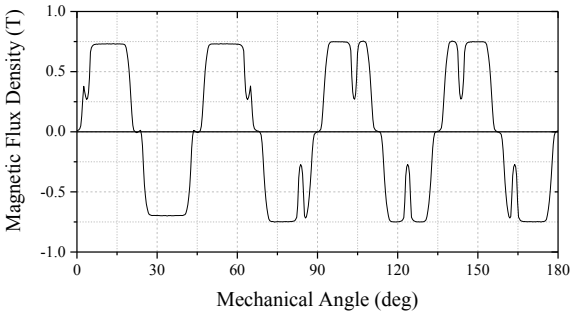

Fig. 3. Magnetic flux density waveform

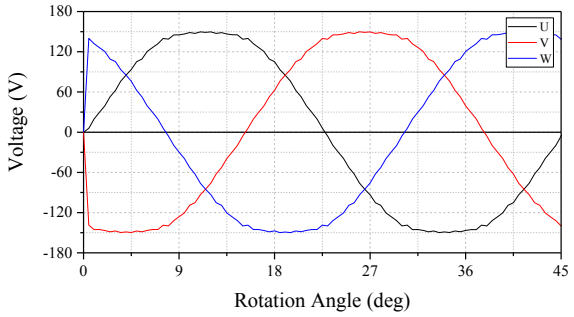

Fig. 4. Back-EMF waveforms

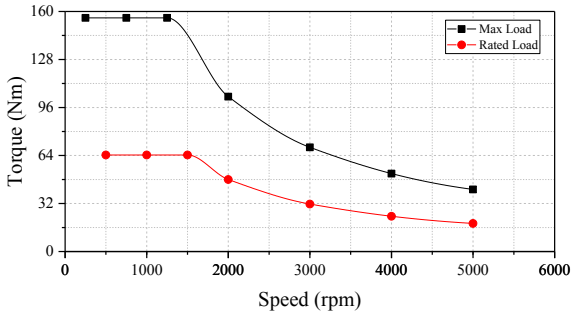

Fig. 5. Output torque versus speed under the max load and rated load

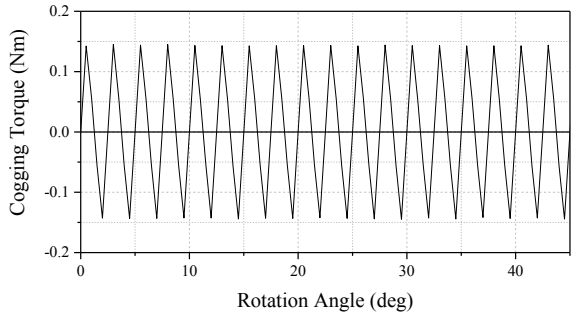

Fig. 6. Cogging torque waveform

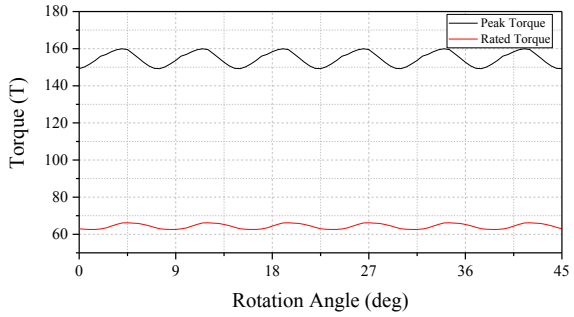

Fig. 7. Peak torque and rated torque waveforms

III. Optimization of Rotor

A. Eccentric arc

Compared with uniform air gap, suitable uneven air gap can effectively improve the air gap flux density waveform [14]. Eccentric arc is a method commonly used to obtain the uneven air gap. As shown in Fig. 8, *oo'* represents the eccentric length and dotted line represents the eccentric arc of one pole. The eccentric length varies from initial 0mm to 40mm at the step of 10mm.

Fig. 9 shows the variation of magnetic flux density waveforms. The results show that the sine characteristic of air gap magnetic flux density gets improved when eccentric length increases. Although the average length of air gap increases, the fundamental amplitude rises slightly due to the decrease of other harmonic contents. Correspondingly, distortion rate of Back-EMF gets lower, as seen in Table IV. In addition, the saliency ratio under the same load is also reduced. As the air

gap length of q-axis increases more than that of d-axis, the q-axis inductance decreases more. As a result, the reluctance torque is reduced. Though the pulsating torque can be suppressed, the output torque decreases at the same time. Fig. 11 and Fig. 12 show the variation of the rated torque and the peak torque.

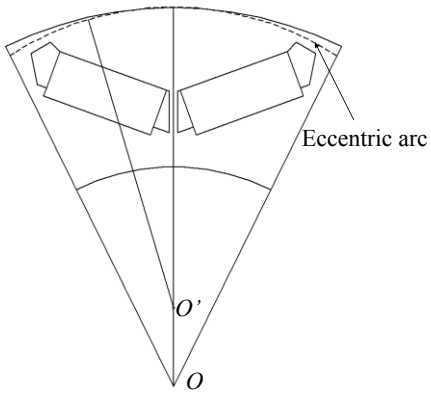

Fig. 8. Diagram of eccentricity

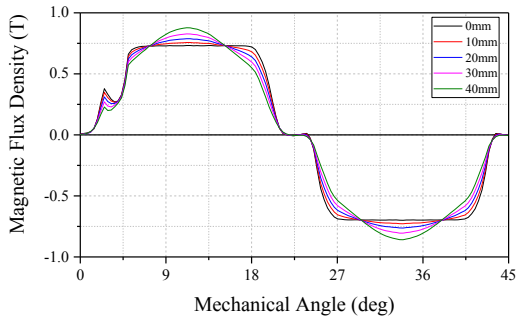

Fig. 9. Comparison of flux density waveforms

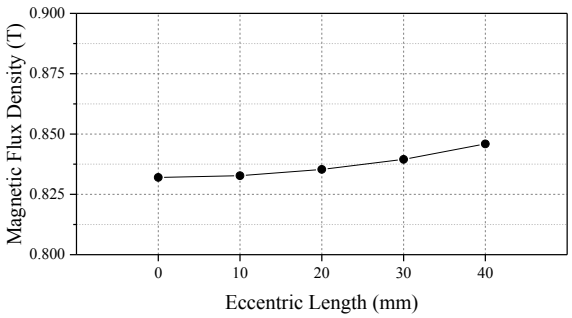

Fig. 10. Fundamental amplitudes of magnetic flux density

TABLE IV. DISTORTION RATES OF BACK-EMF AND Saliency ratios

Eccentric Length	0mm	10mm	20mm	30mm	40mm
Distortion Rate of Back-EMF	1.69%	1.48%	1.27%	1.06%	0.82%
Saliency ratio	1.513	1.475	1.453	1.431	1.405

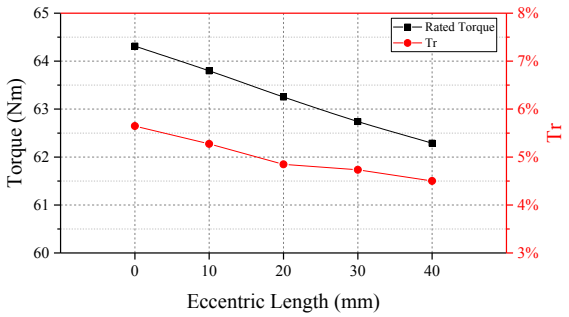

Fig. 11. Rated torque and torque ripple

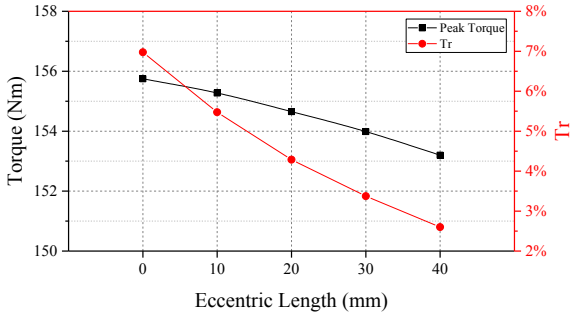

Fig. 12. Peak torque and torque ripple

B. *Angle of pole shoe*

Pole shoe is one of the important components of main flux. Its shape will have certain impacts on the magnetic force line distribution and magnetic filed. This section adjusts the angle of pole shoe, as shown in fig. 13, and compares their performance. The initial value of γ is 17.9° and it varies to 12.9° after six cases.

After finite element analysis, variation of air gap magnetic flux density waveform is shown in Fig. 14. With γ decreasing, flat top of the waveform becomes narrow and amplitude increases gradually. Fig. 15 shows the difference of the fundamental amplitude. Its value also increases. This indicates that smaller γ contributes to producing greater magnet congregate effect. However, the growth trend of flux density is slowing down. With the angle decreasing, the reluctance of the main flux raises. As shown in Fig. 16, the magnetic lines will pass through the air gap inside the magnetic bridge when γ reaches 12.9°. Therefore, too small γ may actually reduce the magnetic flux density due to the excessive increase of reluctance.

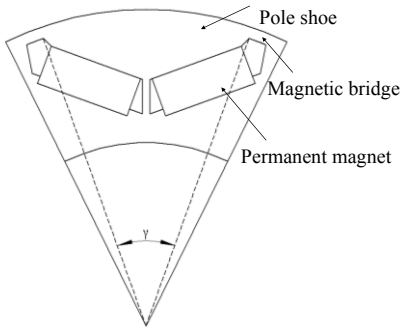

Fig. 13. Diagram of pole shoe angle

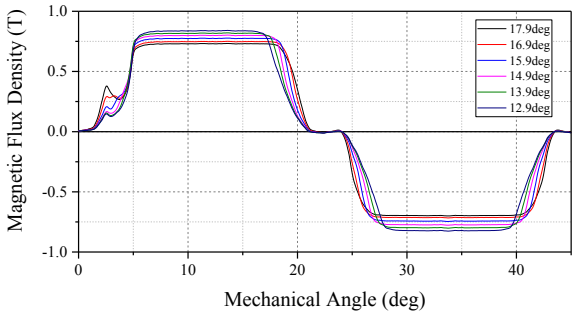

Fig. 14. Comparison of flux density waveforms

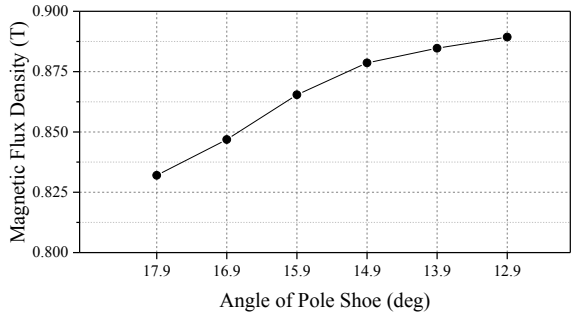

Fig. 15. Fundamental amplitudes of magnetic flux density

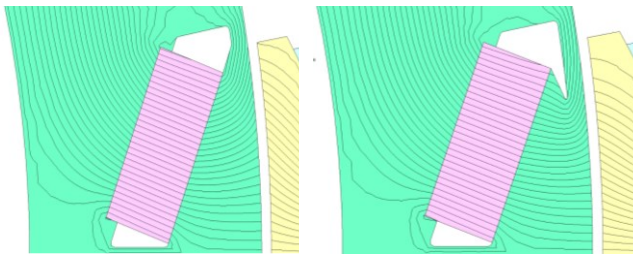

Fig. 16. Comparison of magnetic force line distribution

According to Table V, both the distortion rate of Back-EMF and the saliency ratio increase first and then decrease. Thus, percentage of the pulsating torque under the rated load has the same variation trend, shown in Fig. 17. However, percentage of the pulsating torque keeps declining under the peak load. The main reason may be the variation in magnetic saturation. Furthermore, due to the decrease of reluctance torque, the rated torque and the peak torque both reduce when γ<14.9°, though the air gap magnetic density has been rising.

TABLE V. DISTORTION RATES OF BACK-EMF AND SALIENCY RATIOS

Angle of Pole Shoe	17.9°	16.9°	15.9°	14.9°	13.9°	12.9°
Distortion Rate of Back-EMF	1.69%	1.96%	2.19%	2.28%	2.11%	1.91%
Saliency ratio	1.513	1.519	1.525	1.508	1.493	1.476

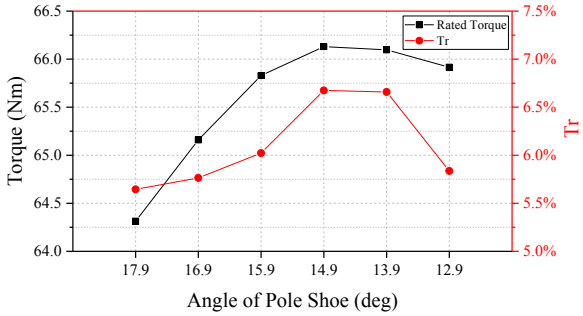

Fig. 17. Rated torque and torque ripple

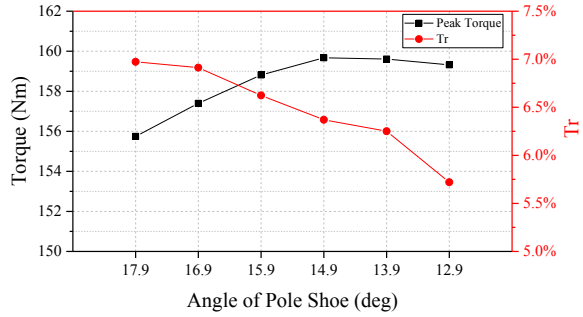

Fig. 18. Peak torque and torque ripple

C. *Optimization Result*

In order to reduce the pulsating torque and avoid excessive reduction of output torque at once, eccentric length is selected to be 30mm and angle of pole shoe is selected to be 15.9°, comprehensively considering their effects on the performance of IPMSM.

Fig. 19 and Fig. 20 show the comparison of magnetic flux density waveforms and Back-EMF waveforms. After optimizing, the fundamental amplitude of flux density reaches 0.86T and the fundamental amplitude of Back-EMF reaches 162.89V. The average peak torque is 156.13Nm and the pulsating torque is 4.88Nm, up to 3.13% of the average peak torque. The average rated torque is 63.84Nm and the pulsating torque is 3.22Nm, up to 5.04% of the average rated torque.

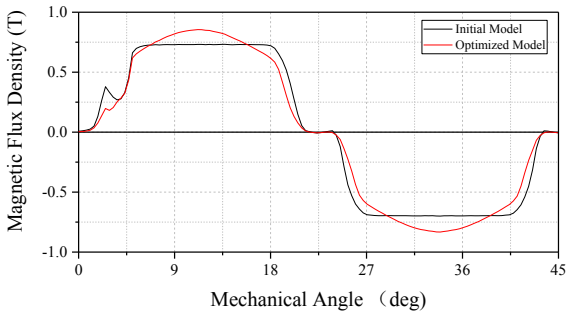

Fig. 19. Comparison of flux density waveforms

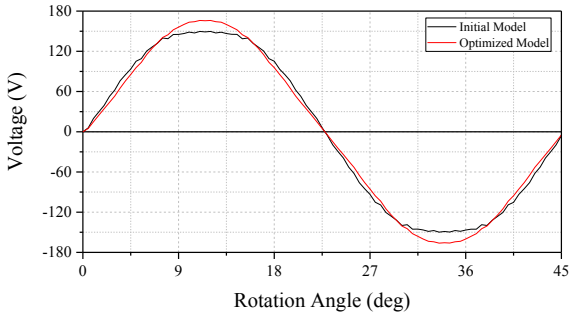

Fig. 20. Comparison of Back-EMF waveforms

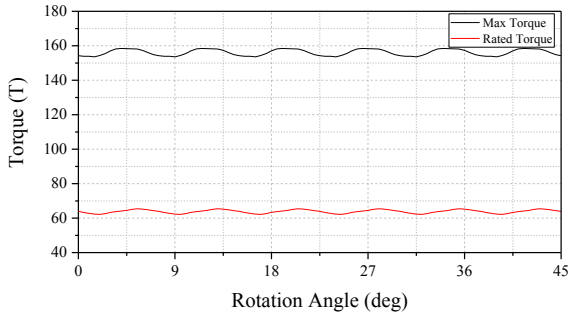

Fig. 21. Peak torque and rated torque waveforms of optimized model

IV. CONCLUSION

This paper presents the design of a FSCW-IPMSM for EVs. The motor has 18 slots and 16 poles. After determining the initial dimensions, the performance of the motor is obtained by finite element analysis. Then rotor structure of the motor is optimized, including the eccentric length and the angle of pole shoe. The eccentric length varies from 0mm to 40mm after five cases and the angle of pole shoe varies from 17.9° to 12.9° after six cases. Comprehensively considering their effects on the performance of IPMSM, the eccentric length is determined to be 30mm and the angle of pole shoe is determined to be 15.9°. After optimizing, torque performance is effectively improved both under the rated load and the peak load.

ACKNOWLEDGMENT

This work is supported by "Six Talents Peak Project of Jiangsu Province" under contract No. XNYQC-CXTD-001 and "the Fundamental Research Funds for the Central Universities" under contract No.30917015101.

REFERENCES

[1] S. J. Lee, S. I. Kim, and J. P. Hong, "Characteristics of PM synchronous motors according to pole-slot combinations for EPS applications," International Journal of Automotive Technology, vol. 15, no. 7, pp. 1183-1187, 2014.

[2] Z. Bin, Q. Ronghai, X.Wei, and L. Jian, "A permanent magnet traction machine with wide high efficiency range for EV application," in Industrial Electronics Society, IECON 2015 - 41st Annual Conference of the IEEE, November 2015, pp. 000457-000463.

[3] B. Aldo, C. Marco, V. Silvio, and D. Thiago, "Thermal conductivity evaluation of fractional-slot concentrated winding machines," in Energy Conversion Congress and Exposition (ECCE), 2016 IEEE, September 2016, pp. 1-7.

[4] EL-Refaie, and M. Ayman, "Fractional-slot concentrated-windings synchronous permanent magnet machines: Opportunities and challenges," Industrial Electronics, IEEE Transactions on, vol. 57, no. 1, pp. 107-121, January 2010.

[5] S. Liwei, J. Daqian, C. Shumei, S. Shan, "Reluctance torque analysis and reactance calculation of IPM for HEVs based on FEM," in Vehicle Power and Propulsion Conference (VPPC), 2010 IEEE, September 2010, pp. 1-4.

[6] O. Junka, S. Masayuki, M. Shigeo, and I. Yukinori, "Influence of magnet and flux barrier arrangement for IPMSM with concentrated winding," in Power Electronics and Drive Systems (PEDS), 2013 IEEE 10th International Conference on, April 2013, pp. 741-745.

[7] W. Daohan, W. Xiuhe, and J. Sang-Yong, "Cogging torque minimization and torque ripple suppression in surface-mounted permanent magnet synchronous machines using different magnet widths," IEEE Transactions on Magnetics, vol. 49, no. 5, pp. 2295-2298, May 2013.

[8] Z. Azar, Z. Q. Zhu, and G. Ombach, "Influence of electric loading and magnetic saturation on cogging torque, back-EMF and torque ripple of PM machines," IEEE Transactions on Magnetics, vol. 48, no. 10, pp. 2650-2658, October 2012.

[9] H. Wenmei, S. Chunyuan, X. Yinlong, S. Guiying, and L. Yuesheng, "Optimal design of permanent magnet linear motor for reducing cogging force ," in Transportation Electrification Asia-Pacific (ITEC Asia-Pacific), 2014 IEEE Conference and Expo, pp. 1-4, November 2014.

[10] K. Gyu-Hong, S. Young-Dae, K. Gyu-Tak and H. Jin, "A novel cogging torque reduction method for interior type permanent magnet motor," IEEE Transactions on Industry Applications, vol. 45, no. 1, pp. 161-167, January/February 2009.

[11] B. Claudio, I. Fabio, L. Emilio, B. Alberto, and D. Matteo, "Review of design solutions for internal permanent-magnet machines cogging torque reduction," IEEE Transactions on Magnetics, vol. 48, no. 10, pp. 2685-2693, October 2012.

[12] W. Zhao, T. A. Lipo, and B.-I. Kwon, "Torque pulsation minimization in spoke-type interior permanent magnet motors with skewing and sinusoidal permanent magnet configurations," IEEE Transactions on Magnetics, vol. 51, no. 11, November 2015.

[13] J. F. Gieras and M. Wing, Permanent Magnet Motor Technology, New York: Marcel Dekker Inc., 2002..

[14] L. Mingji, H. Zhi, P. Yawei, S. Pengfei, "Optimization of permanent magnet motor air-gap flux density based on the non-uniform air gap," in Mechatronic Sciences, Electric Engineering and Computer (MEC), Proceedings 2013 International Conference on, 2013 IEEE, December 2013, pp. 3422-3426.